J. Phys.: Condens. Matter **25** (2013) 094002 (8pp) doi:10.1088/0953-8984/25/9/094002

Exploring highly correlated materials via electron pair emission: the case of NiO/Ag(100)

F O Schumann[1], L Behnke[1], C H Li[1] and J Kirschner[1,2]

[1] Max-Planck Institut für Mikrostrukturphysik, Weinberg 2, D-06120 Halle, Germany
[2] Institut für Physik, Martin-Luther-Universität Halle-Wittenberg, D-06099 Halle, Germany

E-mail: schumann@mpi-halle.de

Received 11 April 2012, in final form 18 June 2012
Published 12 February 2013
Online at stacks.iop.org/JPhysCM/25/094002

Abstract
Metal oxides like NiO are usually termed 'highly correlated', because the material properties are decisively determined by the electron–electron interaction. This makes them interesting candidates for electron pair spectroscopy which is particularly sensitive to the electron correlation. We have prepared ultrathin NiO/Ag(100) films and studied the electron pair emission upon electron impact. Compared to the metal substrate we observe an increase of the coincidence intensity by a factor of 8 for NiO. Thickness dependent measurements prove that this enhancement is an intrinsic effect rather than due to a mean free path increase of the oxide. The Néel temperature T_N of NiO films displays a thickness dependence which allows us to tune T_N. We performed temperature dependent measurements and observed no temperature dependence of the coincidence spectra. This proves that the electron pair emission probes the local correlation rather than long range order. An enhanced coincidence intensity was also found for other oxide phases compared to their corresponding metal phases.

1. Introduction

An important material property of solids is the electric conductivity. It is well known that materials can be insulating, semiconducting or metallic. Therefore the knowledge of the electronic states is important to understand the material properties. A widely used description is the independent electron (quasi-particle) picture, e.g. within the local density approximation (LDA). There the complicated interacting electron system is cast into a model which formally looks as if the electrons are non-interacting. This picture allows a simple criterion for predicting the conduction behavior to be defined. If the highest occupied electron level is separated by an energy gap from the lowest unoccupied level the material is an semiconductor or insulator. If the number of valence electrons per unit cell is odd then the material is a metal. The quasi-particle band structure can be probed via single electron spectroscopy, e.g. photoemission [1, 2]. However, it is also well established that the observed spectra display deviations from the quasi-particle features which are a consequence of the electron–electron interaction [2–13]. A prominent example is the 6 eV satellite from Ni [2, 7, 8]. Other manifestations are rather broad quasi-particle peaks for states below E_F [3–5, 10, 12, 13]. It is interesting to note that the LDA predicts CoO and NiO to be metallic while experimental observations reveal insulating behavior. Clearly an important aspect is missing. It turns out that the electron–electron interaction is not adequately described for these oxidic compounds. The next level of refinement consists in introducing a parameter U which quantifies the energy penalty for double occupancy of a lattice site [14]. This leads to the so-called LDA+U [15] scheme which correctly predicts NiO and CoO to be antiferromagnetic insulators. The need to go beyond the LDA approximation may qualify NiO and CoO as 'highly correlated' systems.

The parameter U has its origin in the Hubbard Hamiltonian. Within this picture a Mott–Hubbard insulator exists for sufficiently strong on-site correlation [14]. We should point out that the classification of NiO as a Mott–Hubbard insulator is not without problems [16–18]. Besides the Ni 3d–3d correlation one has to consider also charge transfer between the NiO 3d and O 2p levels.

According to a scheme proposed by Zaanen, Sawatzky and Allen it is more appropriate to term NiO and CoO as charge transfer insulators [17]. Nevertheless, the Mott–Hubbard picture can be regained for NiO. By this it is meant that the 3d–3d interaction is the relevant many-body term [18]. It is important in the context of this work that the electron correlation for NiO and CoO has to be treated more precisely than in LDA.

A tool which goes beyond the single electron picture is electron pair emission due to electron or photon excitation. This technique is used in atomic, molecular and solid state physics [19–21]. In solids many-body effects are present which have their origin in the electron–electron interaction. Notable examples are long range magnetic order like ferro/antiferromagnetism. Over the last decade we have made significant advances in the instrumentation. So far our studies have concentrated on insulators like LiF, metals and ferromagnetic samples [22–28].

If the excitation is due to primary electrons we speak of an (e, 2e) process. Pair emission due to photon absorption is termed double photoemission (DPE). An obvious choice for further studies is to focus on NiO and CoO specimens, because these materials are usually regarded as 'highly correlated'. Hence, we expect a potentially stronger coincidence signal compared to the previously studied systems. Such a simple picture is supported by a recent theoretical DPE study on a model specimen whose electronic properties are described by a Hubbard Hamiltonian [29]. The key result is a strong dependence of the coincidence intensity on the strength of U. Such a calculation has not been performed for the (e, 2e) process, but due to the similarities in the (e, 2e) and DPE processes it is expected that the intensity enhancement also holds for the (e, 2e) process. This is substantiated by recalling the key features of the current (e, 2e) theory [26, 30–32]. The initial state is described by an LEED state and a Bloch state for the incoming electron and the valence electron, respectively. The outgoing electrons are characterized by time-reversed LEED states. The actual interaction between the electrons is approximated by a screened Coulomb potential, for numerical calculations a Thomas–Fermi screening is employed. The overall structure of the transition probability is given by the matrix elements of this interaction with the initial and final states. Therefore, the strength of the interaction determines the coincidence intensity.

In this work we report on our studies of ultrathin NiO/Ag(100) films. The preparation of NiO films on a Ag(100) substrate is well documented [33–38]. We find an almost one order of magnitude increase of the coincidence intensity compared to the Ag(100) substrate and other metallic films. We investigated the thickness dependence for NiO films and found out that already 2.5 ML NiO/Ag(100) possess more than 60% of the intensity of 15 ML. For this coverage the intensity does not increase with further NiO deposition.

This fact and the overall thickness dependence rule out the possibility that the observed behavior is a result of a large increase of the inelastic mean free path in the insulator compared to metals. We conclude that the intensity increase is an intrinsic effect of the stronger electron correlation in NiO. We find a similar intensity increase for CoO/Ag(100) films compared to the metallic phase.

For a few selected coverages we determined the intensity at 110 and 300 K and found no variation. Recalling the thickness dependence of the Néel temperature T_N for NiO films [39–41], we conclude that the (e, 2e) process probes the local correlation and is independent of the order parameter. Our study also shows that an increased coincidence intensity is related to the increased singles count rate.

2. Experiment

The experiments were performed in a UHV chamber equipped with standard surface science tools. The effect of the Earth's magnetic field was reduced by using external Helmholtz coils and a mu-metal chamber. A sketch of the overall layout of the coincidence experiment is shown in figure 1 which has been described in more detail elsewhere [42–44]. It consists of two hemispherical electron energy analyzers with a mean radius of 200 mm equipped with wide angle transfer lenses and position sensitive detectors [45]. We use channel plate detectors with resistive anodes. We label the spectrometers as 'left' and 'right', respectively. The two electron-optical axes of the spectrometer include an angle of 90° and define the reaction plane, in which the primary electrons with energy E_p and the detectable outgoing electrons with energies E_{left} and E_{right} lie. The angular acceptance of each analyzer is $\pm 15°$ within the scattering plane. All experiments were performed with the primary beam parallel to the normal.

In contrast to the general operation of energy dispersive analyzers, which consists of scanning the kinetic energy of the electrons, we keep all lens voltages fixed for a given primary energy E_p. In this mode of operation, the electrons within an energy window of approximately 8% of the pass energy E_{pass} are detected. An inherent problem of coincidence experiments is the requirement to operate with a low primary flux. The resulting low coincidence rate makes it mandatory to cover an energy window as large as possible while maintaining a reasonable energy resolution. These are conflicting demands, because an increase of the pass energy will lead to a decrease in the energy resolution. As a compromise we performed studies with $E_{pass} = 100$ eV pass energy, hence each spectrometer covers an energy window of 8 eV. The electron gun is equipped with a BaO cathode and the energy spread of the primary beam is ∼0.3 eV[3]. The energy resolution of the coincidence experiments is 0.7 eV as judged from the energy spectra. An advantage of the energy dispersive setup compared to a time-of-flight (TOF) instrument is the ability to record spectra for primary energies up to approximately 100 eV while keeping the energy resolution fixed. This was explored in recent (e, 2e) studies on Cu(111) and Cu(100) surfaces [44, 46]. It is a general observation in our work that the coincidence intensity drops by almost an order of magnitude if E_p is varied from 30 to 100 eV. Additionally, we started to investigate the

[3] Kimball Physics Model ELG-2.

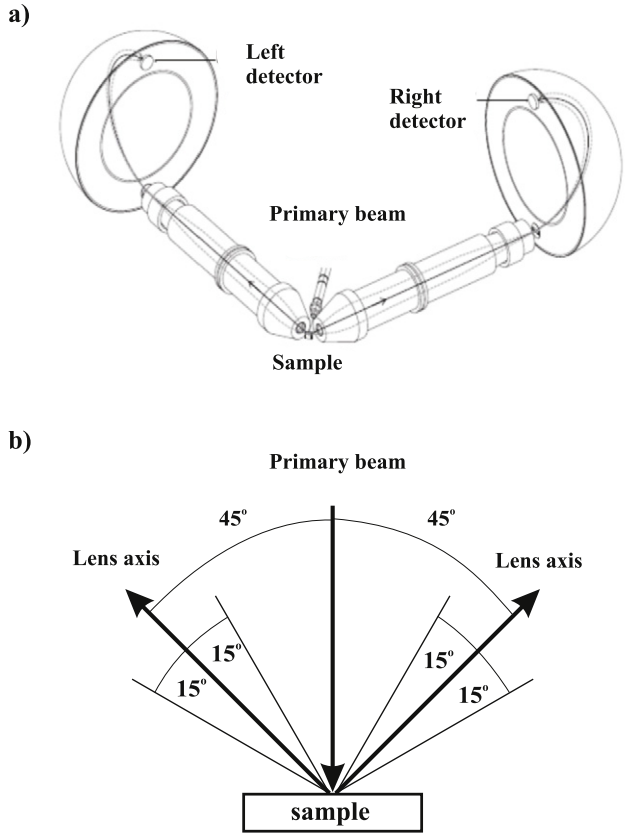

Figure 1. (a) Sketch of the coincidence electron spectrometer. It shows two hemispherical electron energy analyzers that define a scattering plane. (b) The transfer lenses of the spectrometers are symmetrically positioned in the same plane as the primary beam. The outgoing electrons were detected at ±45° with respect to the surface normal. The angular acceptance range of ±15° with respect to mean take off angle is also shown. Only those events which lie in the interval defined by the pair of vertical dashed lines are considered for further analysis.

properties of NiO employing a TOF setup which limits E_p to approximately 30 eV. For higher electron energies the energy resolution due to the time resolution becomes too poor for reasonable studies. Therefore, we limited our studies to $E_p = 31.6$ eV. We employ a four-way coincidence circuit in which the channel plate signals originating from the two spectrometers have to be within a time interval of 100 ns while at the same time the electronics of the resistive anodes indicate a successful impact position determination. If a valid event is registered the arrival times (t_{left} and t_{right}) at the left and right of the detector with respect to the coincidence trigger can be determined. The resulting histogram of the time difference $dt = t_{left} - t_{right}$ of the coincidence intensity will display a peak residing on a constant background [42, 44]. These types of curves play the central role of this work and hence we want to explain them in more detail.

In figure 2 we display a schematic histogram which reflects the typical observation. On the scale of our time resolution the emission of two correlated electrons occurs instantaneously. Therefore the two electrons will be detected at the same time, $dt = 0$. However, the time resolution of the spectrometer is finite and results in a peak width of

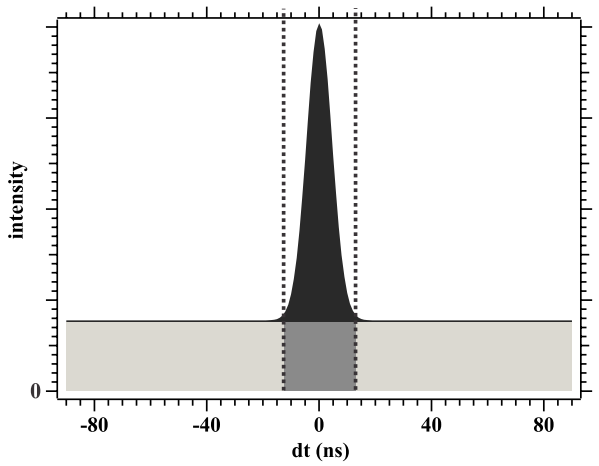

Figure 2. We show a model arrival time $dt = t_{left} - t_{right}$ histogram which reflects typical experimental values. True coincidences show up as a peak residing on a constant background caused by random coincidences, because there is no time correlation between the electrons. The number of random events is given by the gray areas. The number of true coincidences is given by the area of the black peak.

10 ns. This value can be understood to arise mainly due to the differences in transit time in the hemispheres. The time resolution is in accordance with general considerations for a hemispherical analyzer [47] and for the specific model used in our studies [48]. We are interested in the number of so-called true coincidences which are given by the black area in figure 2. Besides those events we will also detect random coincidences due to two independent primary electrons which cause the emission of two uncorrelated electrons. This means that there is no time correlation between these events and we obtain a constant intensity for all dt values. The total intensity for random events is given by the gray areas. Since the total number of counts is measured and the constant intensity level outside the peak region can be easily identified the number of counts in the black region can be directly computed.

In order to obtain energy spectra we select a region near the peak in the dt curve as indicated by the pair of vertical dashed lines. In such a selection the ratio of true to random counts is given by the ratio of the black to the darker gray area. Strictly speaking it is not possible to remove random events from the data set, but the aggregate effect can be removed as explained in the literature [44, 49, 50]. As an example of a 2D-energy distribution we show the result for 15 ML NiO/Ag(100) in figure 3.

The black diagonal line marks the maximum energy the electron pair can have. It is determined by the primary energy and the work function of the sample. These energy distributions will be discussed in a separate work, here we want to focus on the coincidence rate. This is an integration of a 2D-energy spectrum. We kept those settings which resulted in the 2D-energy spectrum in figure 3. Specifically, we set the primary energy to 31.6 eV. We would like to point out that the 2D-energy spectrum in figure 3 shows rather broad features, which are not due to the energy resolution of the experiment but are intrinsic to NiO. From the Ag(100) surface we observe

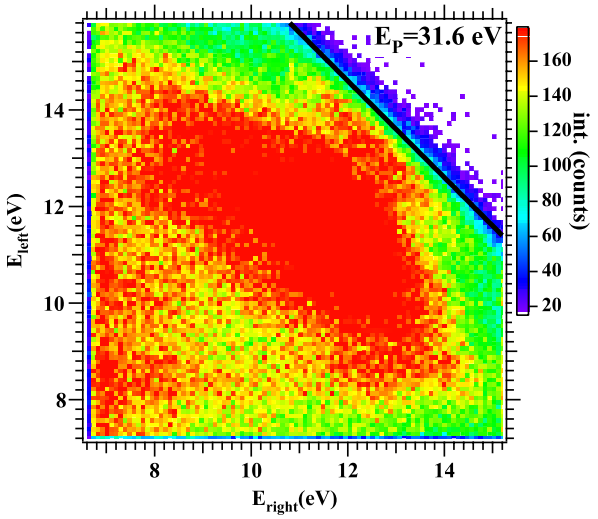

Figure 3. A 15 ML NiO/Ag(100) sample was studied with a primary energy of 31.6 eV. The maximum energy the electron pair can have is marked by the black diagonal line.

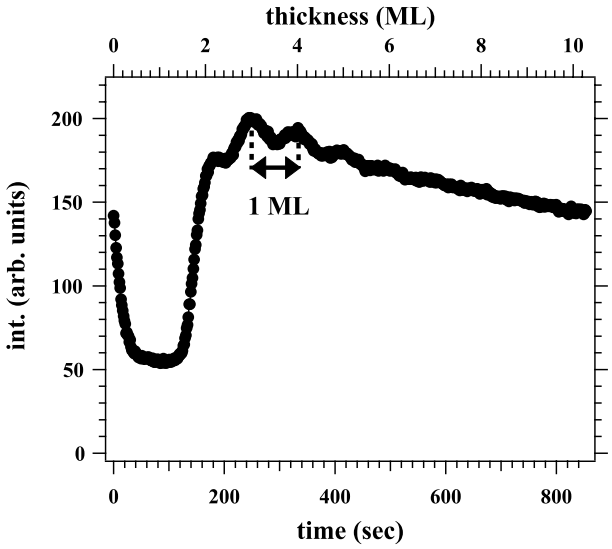

Figure 4. MEED intensity of the specular beam during growth of a NiO/Ag(100) film. The beam energy was 1.5 keV and the sample was kept at room temperature. The oxygen partial pressure was 2×10^{-7} mbar. The oscillation period amounts to the completion of a ML as indicated by the arrow.

finer structures which are similar to the Cu(111) and Cu(100) surfaces as published recently [44, 46].

A recent addition to the experiment is a channel plate detector which can be brought to the sample position. This allows the flux of the incoming primary beam to be determined which is of the order of 2×10^6 electrons s^{-1}. This gave a singles count rate in the range of 3500–7800 cps while the coincidence count rate was 9–13 cps.

The Ag(100) surface was prepared following standard procedures of Ar sputtering and annealing cycles. The experiments were performed at either room temperature or 110 K which constitutes the lowest attainable value of the LN_2 cooling. The base pressure during data acquisition was 4×10^{-11} mbar. All kinetic energies are quoted with respect to the vacuum level of the specimen. The preparation of NiO films followed procedures documented in the literature [33–38, 51]. Specifically, we deposited the NiO film at 300 K in an oxygen atmosphere of 2×10^{-7} mbar. From diffraction measurements during growth we determine a growth rate of 0.8 ML min^{-1}. The preparation of CoO follows the same procedure which also results in a well-ordered structure. Additionally to the oxide films we prepared also polycrystalline Ni and Co films. These were grown on the oxide films; this process does not occur in a layer-by-layer fashion. Via Auger spectroscopy we confirmed that no traces of the underlying film could be seen and we estimated the thickness to be 13–15 ML.

3. Thickness dependence

In the following we will discuss the integral coincidence intensity. As far as thickness control is concerned we employed the MEED intensity variation during growth. This has become a standard tool in thin film growth. In such an experiment a primary electron beam hits the target under a grazing incidence and the diffracted beams are detected on a phosphorous screen. Layer-by-layer growth is manifested by the emergence of intensity oscillations as a function of time. Assuming that a period amounts to 1 ML, a thickness calibration is possible. An example of such behavior during growth of NiO on Ag(100) is depicted in figure 4. This curve was obtained with a primary energy of 1.5 keV and we measured the intensity of the specular reflected beam. The deposition starts at time $t = 0$ and we note that at the beginning of the growth the intensity drops markedly; only at approximately $t = 170$ s is the initial intensity recovered. After this we observe the onset of weak oscillations. We identify the oscillation period as the time required to deposit 1 ML of NiO. The evaluation yields a value of 84 s. With this calibration we can convert the growth time in ML and the result is given as the upper x-axis in figure 4. Our MEED intensity curve is qualitatively in agreement with a recent work although our oscillation amplitude is smaller [51].

Previous STM/STS studies found that in the early stages of the growth a complex behavior exists [35]. Only at coverages above 2 ML was oxidic behavior determined. These growth complications manifest themselves also in stress and structural measurements [51]. We conclude that starting at a coverage of 2 ML NiO we are to expect properties related to a 'highly correlated' material. This coverage can be easily recognized by the MEED intensity curve, see figure 4. The magnetic properties of NiO films have been studied via magnetic linear dichroism studies [39–41]. These measurements provided the thickness dependence of T_N, see table 1. Interestingly, a coverage of 3 ML NiO/Ag(100) revealed a T_N of 390 K [41] while growth on a MgO(100) surface resulted in an ordering temperature below 40 K.

After having demonstrated our ability to control the film thickness we prepared different samples and performed coincidence experiments. From the arrival time histogram curves of the kind presented in figure 2 we can determine the number of true counts as discussed earlier. With the

Table 1. The thickness dependence of NiO films on Ag(100) and MgO(100) surfaces [39–41].

NiO/Ag	NiO/MgO
T_N (3 ML) = 390 K	T_N (3 ML) < 40 K
	T_N (5 ML) = 295 K
	T_N (10 ML) = 430 K
	T_N (20 ML) = 470 K
T_N (30 ML) = 535 K	

known acquisition time we can quote the true coincidence rate. Since the primary flux is known we can finally compute the coincidence intensity per incoming primary electron. In figure 5 we present the thickness dependence of this quantity at 300 K. For some selected NiO films measurements at 110 K were also performed. The thinnest film investigated was 2.5 ML which possesses more than 60% of the intensity of the thickest film. The overall thickness dependence of the coincidence intensity can be described by an exponential behavior with an effective attenuation length of 2.6 ML. This can be corroborated if we consider the attenuation of the primary beam and the attenuation of the two outgoing electrons and the emission geometry. Using recently obtained values for the similar system CoO/Ag(100) in the energy regime of our studies explains our effective attenuation length [52]. Although the mean free paths in metals are significantly shorter than those in CoO [53–56] in the kinetic energy range of this study, this fact is not responsible for the high coincidence intensity for NiO. This can be immediately read from figure 5 where also data points for Ni and Co polycrystalline films are shown. Even the 2.5 ML NiO film has a larger intensity than the metallic films. In figure 5 we also included the intensity value for a 13 ML CoO/Ag(100) film. The coincidence intensity is essentially identical to that of the NiO films. We can clearly see that the intensity levels for NiO and CoO are significantly higher compared to the metallic samples. This point deserves some attention. The very existence of coincidence intensity shows that the electron correlation cannot be neglected in Ni and Co. This does not come as a surprise, because both Ni and Co display ferromagnetic order. This is a macroscopic manifestation of the electron–electron interaction. We may add that a coincidence signal is not tied to ferromagnetic order, because non-magnetic substrates like Cu also display coincidence intensity [27, 44, 46, 57]. The reason why the intensities for Ni and Co are much smaller than those of their oxide counterparts can be understood as follows. Most properties of Ni and Co are well reproduced by a spin-split electronic band structure obtained from an LDA scheme. The Stoner criterion states that ferromagnetism occurs if the density of states at E_F of the paramagnet times the Stoner parameter I exceeds 1. The Stoner parameter I characterizes the tendency to form local magnetic moments which in isolated atoms leads to the Hund rules. For Ni and Co metal the Stoner parameter is of the order of 1 eV [58]. This energy is smaller than the parameter U for NiO and CoO which is 6–7 eV [15]. From this point of view the electron correlation enters on different energy scales for the metal

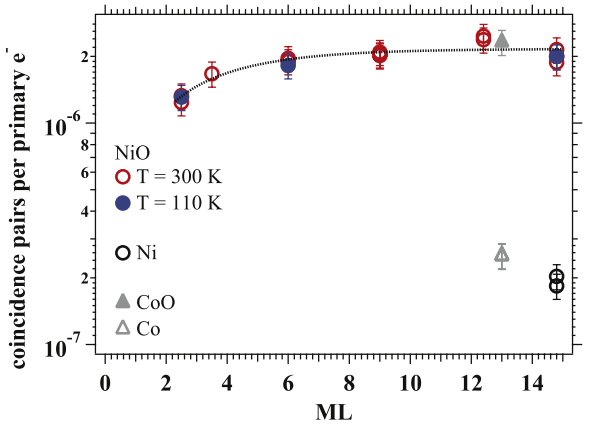

Figure 5. Summary of the coincidence intensity for NiO/Ag(100) films as a function of the thickness. We show the data measured at 300 K (red symbols) and 110 K (blue symbols). The dashed line is a guide for the eye. We have included also the results for a CoO film and for polycrystalline Co and Ni films.

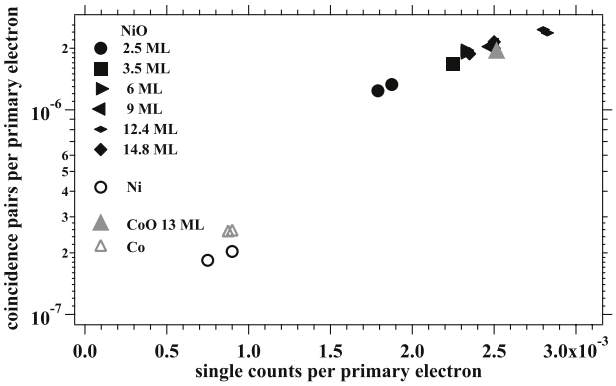

Figure 6. Relation between the singles and coincidence count rates per incoming primary electron. Note the logarithmic scale of the y-axis.

and oxide phases. As discussed in the introduction NiO and CoO can be regarded as 'highly correlated' materials due to the need to include an additional parameter (the Hubbard U) describing the electron correlation. As our experimental technique is particularly sensitive to the electron–electron interaction we observe a strong coincidence intensity. A link between intensity and correlation strength was recently shown to exist in a theoretical study on DPE [29].

In figure 6 we display the coincidence count rate as a function of the singles count rate for a constant primary flux. It is apparent that there is a close relation between these two quantities. A low (high) singles count rate is accompanied by a low (high) coincidence count rate. For example, a 15 ML NiO film has an about a factor of 10 higher coincidence count rate compared to a metallic Ni film. As far as the singles count rate is concerned the 15 ML NiO film has a factor of 3 higher rate than the metallic counterpart.

From this fact alone it is obvious that the pair emission process must be a rather efficient process. This may not be at first sight obvious since of the order 10^6 primary electrons are required to detect a coincidence pair. However, it has

to be remembered that each spectrometer captures only a fraction of the half space. Additionally, the intensity scales with the square of the solid angle of each spectrometer. Using some conservative estimates one comes to the conclusion that 10% of the emitted electrons belong to a pair. From the 2D-energy distribution of figure 3 we learn that we map only those events in which the kinetic energy of the electrons is centered at 11 eV. The width of the energy window is approximately 8 eV. This means that the lowest kinetic energy we detect is 7 eV which is well outside the true secondary peak. Therefore coincidences due to the cascade processes are essentially rejected. We want to emphasize this point by a simple energy argument. The energy required to eject an electron from the highest occupied state into the vacuum region is approximately 4 eV for the metals and the oxide films. This means that for each detected electron we have to provide a minimum energy of 11 eV and the emission of three electrons would require a primary energy of 33 eV. This exceeds the primary energy of $E_p = 31.6$ eV.

4. Temperature dependence

The current theoretical description of the (e, 2e) and DPE processes states that the observable intensity arises from the local correlation. This can be understood within the framework of the exchange–correlation hole [59, 60]. This important concept of solid state theory specifies that each electron is surrounded by a reduced electronic charge density. Furthermore, the integration yields a charge deficit of exactly one elementary charge. This means that the interaction of this electron with other electrons is efficiently screened over distances which are larger than the extension of the exchange–correlation hole. It is commonly assumed that its spatial extension is a few Å. In order to have a finite electron pair emission intensity it is required that the electrons interact which occurs only within close proximity of each other. This fact is implemented by the theoretical description of pair emission via a screened Coulomb interaction with a screening length of a few Å [24, 26]. This quantity does not depend on the temperature which extends to the coincidence intensity too. In particular, no changes are expected if the Néel temperature T_N is exceeded, where the long range magnetic order disappears.

On the other hand, there is clear experimental evidence that the intensity in Auger and photoelectron coincidence studies changes at the Néel temperature for CoO [61, 62]. In this work the MVV Co Auger transition was studied, which involves two valence electrons, in coincidence with the Co 3p photoelectron. The coincidence Auger spectra obtained for the two geometries revealed a difference which vanished once the Néel temperature was crossed. This observation was ascribed to a collapse of the short range order at T_N.

From this point of view it is important to determine whether the (e, 2e) process displays a dependence on the order parameter in order to check the current (e, 2e) theory. As far as the Néel temperature of NiO films is concerned, we recall linear dichroism experiments which studied the $T_N(d)$ behavior of NiO films on MgO(100) and Ag(100)

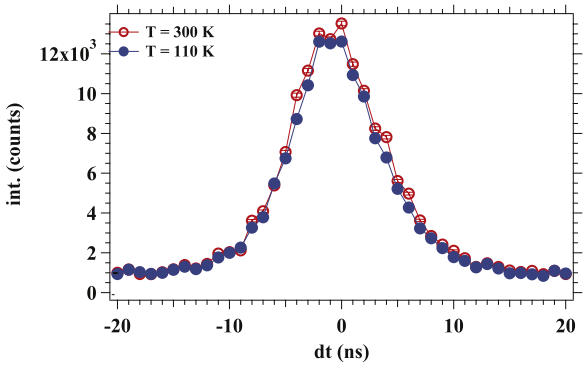

Figure 7. The arrival time histogram is shown for a 6 ML thick NiO/Ag(100) film. The measurements were performed at either 300 or 110 K. The data acquisition time for each spectrum was 1 h.

substrates [39–41]; we compiled these data into table 1. The general trend is that the Néel temperature increases with thickness as observed for many ferromagnetic thin film systems. Interestingly, the choice of the substrate plays an important role for the thinnest films (3 ML) studied. While on a Ag(100) substrate a critical temperature of 390 K is reported, the same thickness deposited on a MgO(100) substrate has a T_N value below 40 K. It is important to realize that a thickness dependent measurement at a constant temperature (e.g. 300 K) is effectively a temperature dependent measurement. If the ordering temperature plays a role we have to expect a signal increase additionally to the exponential increase. Inspection of figure 5 reveals that this is not the case. This is a first hint that the (e, 2e) process does not probe long range order. We studied selected thicknesses at 300 and 110 K and as an example we present the *dt*-spectrum for 6.5 ML NiO/Ag(100) film at 300 K (red symbols) and 110 K (blue symbols), see figure 7. It is apparent that there exists no discernable difference between the two curves. Since the data acquisition time, which was 1 h, and all other experimental parameters were kept constant one can directly compare the two curves. We also studied a 2.5 ML thick film which should have an ordering temperature below 390 K. Due to the known rapid increase of the critical temperature in ferromagnetic films in this thickness regime we can expect T_N to be within the temperature interval of 110–300 K. Our experimental result is that the coincidence intensity of this film does not differ for measurements at 110 and 300 K. The result of measurements at 110 K has been included in figure 5. We conclude that the (e, 2e) intensity does not depend on the temperature even in the vicinity of T_N. This confirms that (e, 2e) probes the local correlation as assumed by the current (e, 2e) and DPE theory.

5. Summary

We found that the coincidence intensity for NiO is an order of magnitude higher than those from the substrate, Ni and Co polycrystalline films. Already 2.5 ML NiO/Ag(100) displays a stronger signal than those of the Co and Ni films which rules out the influence of an increased mean free path for insulators. We interpret our measurements as evidence that

the pair emission intensity scales with the electron–electron interaction strength. Such a behavior was predicted for double photoemission.

We find that there exists a relation between the singles and coincidence rates; the strong variations we observe can only be understood if we assume that the pair emission process is a likely event to occur. We estimate that 10% of all electrons emitted form a pair.

We demonstrate that the coincidence intensity is not influenced by the ordering temperature. This proves that (e, 2e) is an experiment which probes the local correlation and is not sensitive to any long range order. This confirms an important assumption of the current (e, 2e) and DPE theory.

Acknowledgments

We thank Y Pavlyukh and J Berakdar for stimulating discussions. Financial support from the DFG through SFB 762 is gratefully acknowledged.

References

[1] Feuerbacher B, Fitton B and Willis R F (ed) *Photoemission and the Electronic Properties of Surfaces* (New York: Wiley)
[2] Hüfner S 2003 *Photoelectron Spectroscopy* (Berlin: Springer)
[3] Monastra S, Manghi F, Rozzi C A, Arcangeli C, Wetli E, Neff H-J, Greber T and Osterwalder J 2002 *Phys. Rev. Lett.* **88** 236402
[4] Sánchez-Barriga J *et al* 2009 *Phys. Rev. Lett.* **103** 267203
[5] Sánchez-Barriga J *et al* 2010 *Phys. Rev.* B **82** 104414
[6] Clauberg R, Gudat W, Kisker E, Kuhlmann E and Rothberg G M 1981 *Phys. Rev. Lett.* **47** 1314
[7] Guillot C, Ballu Y, Paigné J, Lecante J, Jain K P, Thiry P, Pinchaux R, Pétroff Y and Falicov L M 1977 *Phys. Rev. Lett.* **39** 1632
[8] Eberhardt W and Plummer E W 1980 *Phys. Rev.* B **21** 3245
[9] van der Laan G, Surman M, Hoyland M A, Flipse C F J, Thole B T, Seino Y, Ogasawara H and Kotani A 1992 *Phys. Rev.* B **46** 9336
[10] Manghi F, Bellini V, Osterwalder J, Kreutz T, Aebi P and Arcangeli C 1999 *Phys. Rev.* B **59** R10409
[11] van der Laan G, Zaanen J, Sawatzky G A, Karnatak R and Esteva J-M 1986 *Phys. Rev.* B **33** 4253
[12] Valla T, Fedorov A V, Johnson P D and Hulbert S L 1999 *Phys. Rev. Lett.* **83** 2085
[13] Braun J, Minár J, Ebert H, Katsnelson M I and Lichtenstein A I 2006 *Phys. Rev. Lett.* **97** 227601
[14] Hubbard J 1963 *Proc. R. Soc.* A **276** 238
[15] Anisimov V I, Zaanen J and Andersen O K 1991 *Phys. Rev.* B **44** 943
[16] Hüner S, Steiner P, Sander I, Neumann M and Witzel S 1991 *Z. Phys.* B **83** 185
[17] Zaanen J, Sawatzky G A and Allen J W 1985 *Phys. Rev. Lett.* **55** 418
[18] Manghi F, Calandra C and Ossicini S 1994 *Phys. Rev. Lett.* **73** 3129
[19] Avaldi L and Huetz A 2005 *J. Phys. B: At. Mol. Opt. Phys.* **38** S861
[20] Ullrich J, Moshammer R, Dorn A, Dörner R, Schmidt L P H and Schmidt-Böcking H 2003 *Rep. Prog. Phys.* **66** 1463
[21] Berakdar J and Kirscher J (ed) 2004 *Correlation Spectroscopy of Surfaces, Thin Films, and Nanostrucutures* (Weinheim: Wiley)
[22] Schumann F O, Kirschner J and Berakdar J 2005 *Phys. Rev. Lett.* **95** 117601
[23] Schumann F O, Winkler C, Kerherve G and Kirschner J 2006 *Phys. Rev.* B **73** 041404
[24] Fominykh N, Berakdar J, Henk J and Bruno P 2002 *Phys. Rev. Lett.* **89** 086402
[25] Schumann F O, Winkler C and Kirschner J 2009 *Phys. Status Solidi* b **246** 1483
[26] Berakdar J, Gollisch H and Feder R 1999 *Solid State Commun.* **112** 587
[27] Schumann F O, Winkler C and Kirschner J 2007 *Phys. Rev. Lett.* **98** 257604
[28] Schumann F O, Winkler C, Kirschner J, Giebels F, Gollisch H and Feder R 2010 *Phys. Rev. Lett.* **104** 087602
[29] Napitu B D and Berakdar J 2010 *Phys. Rev.* B **81** 195108
[30] Gollisch H, Yi X, Scheunemann T and Feder R 1999 *J. Phys.: Condens. Matter* **11** 9555
[31] Gollisch H, Schwartzenberg N v and Feder R 2006 *Phys. Rev.* B **74** 075407
[32] Giebels F, Gollisch H, Feder R, Schumann F O, Winkler C and Kirschner J 2011 *Phys. Rev.* B **84** 165421
[33] Peacor S and Hibma T 1994 *Surf. Sci.* **301** 11
[34] Wollschläger J, Erdös D, Goldbach H, Höpken R and Schröder K M 2001 *Thin Solid Films* **400** 1
[35] Grosser S, Hagendorf C, Neddermeyer H and Widdra W 2008 *Surf. Interface Anal.* **40** 1741
[36] Caffio M, Cortigiani B, Rovida G, Atrei A, Giovanardi C, di Bona A and Valeri S 2003 *Surf. Sci.* **531** 368
[37] Marre K and Neddermeyer H 1993 *Surf. Sci.* **287/288** 995
[38] Marre K, Neddermeyer H, Chassé A and Rennert P 1996 *Surf. Sci.* **357/358** 233
[39] Alders D *et al* 1995 *Europhys. Lett.* **32** 259
[40] Alders D, Tjeng L H, Voogt F C, Hibma T, Sawatzky G A, Chen C T, Vogel J, Sacchi M and Iacobucci S 1998 *Phys. Rev.* B **57** 11623
[41] Altieri S *et al* 2009 *Phys. Rev.* B **79** 174431
[42] van Riessen G A, Schumann F O, Birke M, Winkler C and Kirschner J 2008 *J. Phys.: Condens. Matter* **20** 442001
[43] van Riessen G A, Wei Z, Dhaka R S, Winkler C, Schumann F O and Kirschner J 2010 *J. Phys.: Condens. Matter* **22** 092201
[44] Schumann F O, Dhaka R S, van Riessen G A, Wei Z and Kirschner J 2011 *Phys. Rev.* B **84** 125106
[45] Mårtensson N, Baltzer P, Brambilla A, Brühwiler P A, Forsell J O, Nilsson A, Stenborg A and Wannberg B 1994 *J. Electron. Spectrosc. Relat. Phenom.* **70** 117
[46] Wei Z, Schumann F O, Dhaka R S and Kirschner J 2012 *Phys. Rev.* B **85** 195120
[47] Völkel M and Sandner W 1983 *J. Phys. E: Sci. Instrum.* **16** 456
[48] Kugeler O, Marburger S and Hergenhahn U 2003 *Rev. Sci. Instrum.* **74** 3955
[49] Sawatzky G A 1988 Auger photoelectron coincidence spectroscopy *Auger Electron Spectroscopy* ed R P Messmer and C L Bryant (San Diego, CA: Academic)
[50] Jensen E, Bartynski R A, Hulbert S L and Johnson E D 1992 *Rev. Sci. Instrum.* **63** 3013
[51] Dhaka A, Sander D, Meyerheim H L, Mohseni K, Soyka E, Kirschner J, Adeagbo W A, Fischer G, Ernst A and Hergert W 2011 *Phys. Rev.* B **84** 195441
[52] Offi F, Iacobucci S, Vilmercati P, Rizzo A, Goldoni A, Sacchi M and Panaccione G 2008 *Phys. Rev.* B **77** 201101

[53] Ertl G and Küppers J 1985 *Low Energy Electrons and Surface Chemistry* (Weinheim: VCH Verlag)
[54] Pappas D P, Kämper K P, Miller B P, Hopster H, Fowler D E, Brundle C R, Luntz A C and Shen Z X 1991 *Phys. Rev. Lett.* **66** 504
[55] Passek F, Donath M and Ertl K 1996 *J. Magn. Magn. Mater.* **159** 103
[56] Getzlaff M, Bansmann J and Schönhense G 1993 *Solid State Commun.* **87** 467
[57] Herrmann R, Samarin S, Schwabe H and Kirschner J 1998 *Phys. Rev. Lett.* **81** 2148
[58] Janak J F 1977 *Phys. Rev.* B **16** 255
[59] Wigner E and Seitz F 1933 *Phys. Rev.* **43** 804
[60] Slater J C 1934 *Rev. Mod. Phys.* **6** 209
[61] Gotter R, Offi F, Ruocco A, Da Pieve F, Bartynski R, Cini M and Stefani G 2011 *Europhys. Lett.* **94** 37008
[62] Cini M, Perfetto E, Gotter R, Offi F, Ruocco A and Stefani G 2011 *Phys. Rev. Lett.* **107** 217602